nature biotechnology



# Cell-specific targeting of nanoparticles by multivalent attachment of small molecules

Ralph Weissleder[1], Kimberly Kelly[1,2], Eric Yi Sun[1,2], Timur Shtatland[1] & Lee Josephson[1]

**Nanomaterials with precise biological functions have considerable potential for use in biomedical applications. Here we investigate whether multivalent attachment of small molecules can increase specific binding affinity and reveal new biological properties of such nanomaterials. We describe the parallel synthesis of a library comprising 146 nanoparticles decorated with different synthetic small molecules. Using fluorescent magnetic nanoparticles, we rapidly screened the library against different cell lines and discovered a series of nanoparticles with high specificity for endothelial cells, activated human macrophages or pancreatic cancer cells. Hits from the last-mentioned screen were shown to target pancreatic cancer *in vivo*. The method and described materials could facilitate development of functional nanomaterials for applications such as differentiating cell lines, detecting distinct cellular states and targeting specific cell types.**

One of the emerging goals of nanotechnology is to functionalize inert and biocompatible materials to impart precise biological functions. Several novel materials have recently been described for diagnostic or therapeutic use[1–3], including quantum dots[4–6], polymers[7,8] and magnetofluorescent nanoparticles[9,10]. Considerable effort has been directed toward rational surface modifications and coatings to modulate pharmacokinetic properties (e.g., blood half-life, elimination and biodegradation), toxicity, immunogenicity and efficient targeting. Targeting has generally been achieved by conjugating nanoparticle surfaces to antibodies. Although this approach has succeeded for *in vitro* sensing[11,12], its *in vivo* application has proved more challenging because of cost, limited shelf life, regulatory hurdles and potential immunogenicity after repeat injections of such preparations[13]. Another targeting approach with promising initial results involves conjugation of nanoparticles to peptides[14,15] but synthetic costs can be high.

To take advantage of a more diverse chemical space, we hypothesized that small-molecule modifications could change the biological properties of nanoparticles and thereby permit site-specific targeting through small molecule–mediated multivalent binding to cell-surface receptors. To date, the potential of such small-molecule approaches for the design of nanoparticle surfaces has not been realized, primarily because of a lack of a general method to modify surfaces rapidly, to characterize these modified surfaces chemically and to rapidly screen the resulting nanomaterials for biological activity.

Here we describe the creation of a small-molecule nanoparticle library for the rapid development of magnetofluorescent reporters. We show that a union between nanotechnology and small-molecule chemistry can facilitate development of a wide range of nanomaterials for biomedical applications. Specifically, we screened a model nanoparticle library against different cell lines and states. We identified nanomaterials that discriminate among distinct cell types, or among different physiological states of a given cell type.

## RESULTS

### Synthesis of nanoparticle library

The first step towards creation of the nanoparticle library was to identify biologically and chemically suitable nanoparticles that could be detected by magnetic and fluorescent means and could be chemically modified. We used magnetofluorescent nanoparticles[9,10] as starting material because such preparations can be made with high ($R2 > 30$ mMsec$^{-1}$) magnetic relaxivity, because related materials are biocompatible and in clinical use[16], and because aminated base materials facilitate conjugation of small molecules through sulfhydryl, carboxyl, amine and anhydride chemistries (**Fig. 1e**).

Using a modified robotic system, we conjugated 146 different small molecules to nanoparticles in array format. Previous feasibility studies had identified several classes of small molecules that combine water solubility, conjugatability, biocompatibility and chemical diversity. In general, we focused on small molecules (MW $<$ 500 Da) with the chemical functional groups of primary amines, alcohols, carboxylic acids, sulfhydryls and anhydrides (**Fig. 1** and **Supplementary Table 1** online), and excluded compounds known to bind proteins. On average, 60 small molecules were attached per 38-nm nanoparticle. All synthesized and purified nanoparticles were water-soluble, magnetic and fluorescent (**Fig. 1d**) and could be stored for prolonged periods. Nanoparticle libraries were stored in multiwell plates until use in cell-based high-throughput screens.

### Screening identifies unique nanoparticles

We next tested the nanoparticle library for its effects on mammalian cells. We were particularly interested in whether small-molecule

[1]Center for Molecular Imaging Research, Massachusetts General Hospital, Harvard Medical School, Bldg. 149, 13th Street, Room 5403, Charlestown, Massachusetts 02129, USA. [2]These authors contributed equally to this work. Correspondence should be addressed to R.W. (weissleder@helix.mgh.harvard.edu).

Received 24 March; accepted 29 September; published online 23 October 2005; doi:10.1038/nbt1159

surface modification can be used to: (i) change the cellular affinity of nanoparticles, (ii) develop materials that discriminate among closely related functional states of cells, for example, resting and activated (disease-associated) macrophages, (iii) develop disease-specific targeting agents without prior knowledge of a specific target and (iv) develop more efficiently targeted nanomaterials.

**Figure 2** summarizes the results of over 30 screening experiments. The heat map represents the log of mean cellular uptake of different nanoparticles in five different cell types. Human umbilical vein endothelial cells (HUVEC), primary resting human macrophages, granulocyte macrophage colony stimulating factor (GM-CSF)–stimulated human macrophages, a U937 human macrophage-like cell line and human pancreatic ductal adenocarcinoma cells were all probed in quadruplicate. Each row represented a different nanoparticle preparation. Cellular uptake varied over three orders of magnitude (red, low; green, high) ranging from 2–2,239 fg Fe/cell. Notably, there was substantial diversity in cellular uptake among the different nanoparticle compounds, both within a given cell type and among different cell types. For example, for the human pancreatic cancer cell line PaCa-2, uptake varied from 3–1,065 fg Fe/cell among the different preparations ($1.1 \times 10^4$ – $5.5 \times 10^6$ nanoparticles per cell). Compared to monocrystalline iron oxide nanoparticle (MION), a prototype clinical preparation, several small-molecule modifications (e.g., iodoacetic anhydride, diaminopropane or diethylenetriamine) showed much lower macrophage uptake, an important consideration for improving *in vivo* targeting. We also noted a considerable difference in cellular uptake between resting and GM-CSF–stimulated human macrophages in the primary screen (**Fig. 2**).

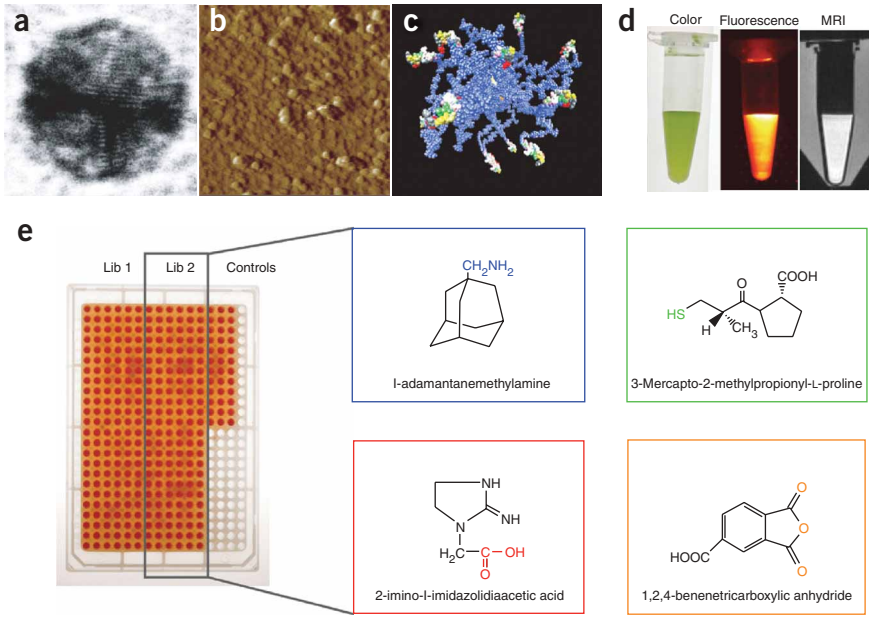


**Figure 1** Nanoparticle and derived-nanoparticle library. (**a**,**b**) Laser light scattering (**a**) and atomic force microscopy (**b**) were used to reveal nanoparticles (38 nm mean diameter) comprising a magnetic core and surface-bound, crosslinked dextran. (**c**) Model of the crosslinked dextran coating modified with small molecules. (**d**) The nanoparticles are fully soluble in water, are fluorescent and superparamagnetic, that is, detectable by magnetic resonance imaging (MRI). (**e**) Different classes of small molecules with amino, sulfhydryl, carboxyl or anhydride functionalities were anchored onto the nanoparticles and stored in multiwell plates for testing.

## Cell-based phenotyping

To examine whether macrophage activation status could indeed be probed with selected materials, we scaled up the synthesis of two nanoparticle preparations (CLIO-bentri and CLIO-gly) identified through the primary screen. Primary isolated human macrophages were cultured for 7 d and stimulated with GM-CSF (to simulate macrophages in immune disease), oxidized low density lipoprotein (LDL) (to simulate foam cells found in atherosclerosis[17]) or lipopolysaccharide (LPS) (to simulate macrophages in infection). CLIO-bentri (compound 261-14-1, **Supplementary Table 1**) was by far the preferred compound internalized into resting macrophages, with uptake higher than the parent compound CLIO-$NH_2$, whereas CLIO-gly (compound 261-47-1, **Supplementary Table 1**) was the preferred compound for activated macrophages (for all three activation methods—GM-CSF, ox-LDL, LPS) as determined by epifluorescence and confocal microscopy (**Fig. 3**). Interestingly, the starting material CLIO-$NH_2$ showed no apparent preference among the cell populations. These compounds (**Fig. 2**) are promising candidates for developing more efficient agents for treating autoimmune diseases[18] or detecting vulnerable atherosclerotic plaques[19].

Based on these screening results, we next investigated whether small-molecule modification can impart unique biological functions to nanoparticles. Molecularly targeted nanomaterials show promise for visualizing specific targets *in vivo* and for delivering therapies. Cell-internalizing affinity ligands are often used to improve target-to-background ratios[15,20]. We hypothesized that this and other amplification strategies could be further enhanced by decreasing nonspecific macrophage uptake of nanoparticles through modification of their surfaces. After identifying unique nanoparticles with low macrophage uptake (**Fig. 2**), we asked whether iodoacetate surface modification (shown above to reduce macrophage uptake) could improve target-to-macrophage ratios conferred by a VCAM-1 targeting peptide sequence (VHSPNKK)[15]. **Figure 4** compares cellular uptake into VCAM-1–positive murine heart endothelial cells (MHEC) and nonspecific uptake into VCAM-1–negative murine macrophages. *In vivo* targeting of activated VCAM-1–expressing endothelial cells present in macrophage-rich diseases such as atherosclerosis requires a reduction in nonspecific nanoparticle phagocytosis into macrophages. As expected, peptide attachment via the C-terminal carboxylate to the unmodified CLIO nanoparticle increased uptake into MHEC, but there was also high uptake into macrophages. Iodoacetic anhydride modification of the peptide-conjugated nanoparticle greatly decreased macrophage uptake. This caused a tenfold improved target-to-background ratio, confirming cellular uptake results. Similar results were also observed for other small molecules that decreased macrophage uptake (**Fig. 2**).

## *In vivo* imaging

We next determined whether the library could be used to identify compounds that preferentially targeted cancer cells but had concomitantly low uptake in macrophages and endothelial cells. Given the

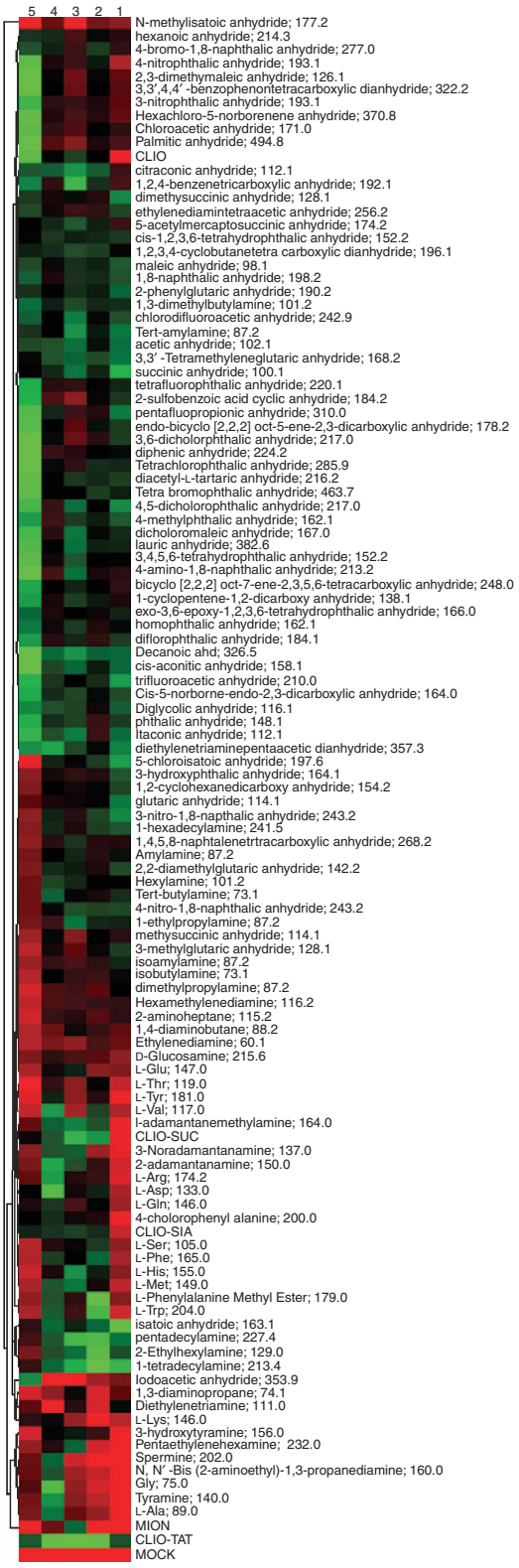


**Figure 2** Heat map representing cellular uptake of different nanoparticle preparations. Columns from right to left: 1, pancreatic cancer cells (PaCa-2); 2, macrophage cell line (U937); 3, resting primary human macrophages; 4, activated primary human macrophages; 5, human umbilical vein endothelial cells (HUVEC). Each column represents mean values from six different experiments. Red refers to the lowest accumulation and green refers to the highest accumulation.

lack of efficient molecules for early detection of pancreatic cancer, we selected PaCa-2 cells from this tumor-type as a model system (**Fig. 2**). Fourteen compounds showed significant uptake into these cancer cells (up to 160 × $10^6$ nanoparticles per cell for the most efficient compounds).

Of these compounds, two (isatoic anhydride, 261-15-28 and 5-chloro-isatoic anhydride, 261-14-17) exhibited high cancer cell uptake and low macrophage/endothelial cell uptake. These compounds were scaled up for *in vivo* use and shown to facilitate pancreatic cancer detection in a mouse model (**Fig. 5**). Simultaneous injection of CLIO-$NH_2$-Cy3.5 and CLIO-isatoic-Cy5.5 into tumor-bearing mice significantly increased fluorescence of CLIO-isatoic-Cy5.5 versus CLIO-$NH_2$-Cy3.5 (TBR 1.63 vs. 0.16, $P < 0.0001$) as determined by fluorescence imaging. These findings were corroborated by fluorescence microscopy showing widespread accumulation of targeted nanoparticles within tumor cells, indicating access to the tumor interstitium through capillaries. Additional *in vivo* experiments demonstrated that the signal in the Cy5.5 channel arose primarily from targeting and not from enhanced photon propagation at different wavelengths. **Figure 6** shows *in vivo* targeting in different channels depending on different fluorochromes covalently attached to CLIO-isatoic.

To verify the fluorescent screening data, we also conducted quantitative biodistribution experiments with $^{111}$In-labeled nanoparticles, bearing in mind that further diethylene triamine pentaacetic acid modification might mitigate isatoic-mediated targeting effects (**Fig. 5**). A higher uptake of the targeted nanoparticle preparation was seen in pancreatic cancer cells (3.7 ± 0.14 injected dose (ID)/g for CLIO-isatoic versus 2.2 ± 0.39 ID/g for CLIO-$NH_2$, $P < 0.0001$; **Fig. 5**), whereas uptake in liver (40.4 ± 5.3 ID/g for CLIO-isatoic versus 40.2 ± 3.6 ID/g for CLIO-$NH_2$), lung, muscle and other organs was similar for both preparations (**Fig. 5**). Enhanced uptake in liver is commonly observed with carbohydrate-modified nanoparticle preparations because of the efficient uptake mechanism into cells of the reticuloendothelial system and the large blood volume and high perfusion of the liver. Although this may pose limitations to *in vivo* imaging (particularly with isotope- and fluorochrome-labeled nanoparticles), it may be less of a problem with spatially resolved techniques such as magnetic resonance imaging. It is conceivable that library approaches similar to the one described here may be used to discover compounds with lower liver accumulation. Overall, these results indicate that small-molecule modification can indeed impart unique functions to nanoparticles and facilitate *in vivo* targeting.

## DISCUSSION

We have applied a magnetofluorescent nanoparticle library decorated with small molecules to address four critical questions in biomedical nanomaterial research: (i) Is it possible to modulate the relative affinity of nanoparticles for different cell types through small-molecule surface modification? (ii) Can small-molecule surface modification be used to discriminate between closely related functional states of cells? (iii) Can affinity tag–conjugated nanomaterials be made more efficient by reducing macrophage uptake? and (iv) Can disease-specific nanoparticles be developed without a priori knowledge of the target? We show several proof-of-principle examples attesting to the ability of small-molecule modifications to address these questions. Screening of this library identified a variety of nanomaterials that discriminate among different cell types as well as among different physiologic states of the same cell type. We envision that similar high-throughput screens could facilitate other tasks such as identifying the effects of nanomaterials on cell differentiation[21], toxicity[22] and pharmacokinetics. Furthermore, attachment of small molecules to magnetofluorescent

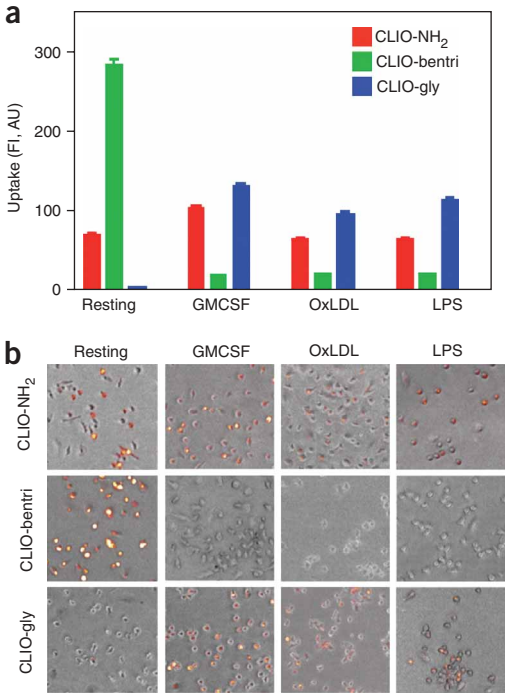


**Figure 3** Nanoparticle 'hits' identified from the large screen (**Fig. 2**) were probed against resting and activating macrophages. (**a**) Quantitative fluorescence-activated cell sorting (FACS) analysis from three separate experiments. (**b**) Epifluorescence microscopy with 680-nm channel (CLIO-Cy5.5) merged onto phase contrast images. Note the preference of CLIO-bentri for resting macrophages and CLIO-gly for activated macrophages. Notably, the starting material CLIO-NH2 shows no apparent preference among the cell populations (mean ± s.d.). GM-CSF, granulocyte macrophage colony; stimulating factor; Ox-LDL, oxidized low density lipoprotein; LPS, lipopolysaccharide. Scale bar, 10 μm.

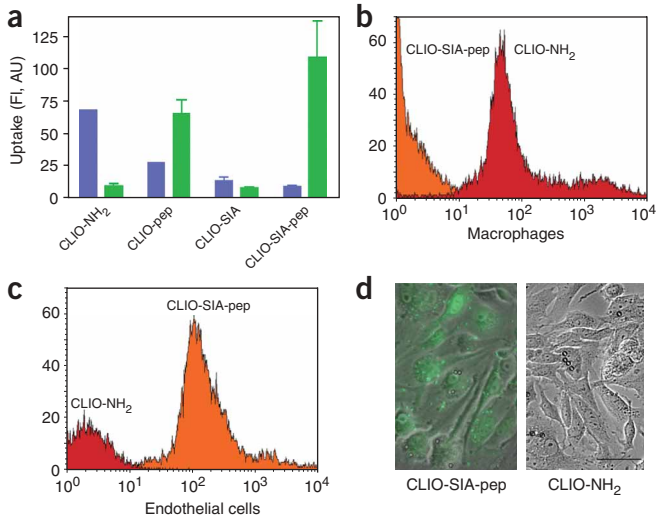


**Figure 4** Targeting experiments. (**a**) Cellular uptake of different nanoparticle preparations into macrophages lacking VCAM-1 (blue) or murine heart endothelial cells (MHEC) expressing VCAM-1 (green). The starting material CLIO-$NH_2$ shows a preferential affinity for macrophages, whereas SIA modification decreases macrophage affinity. VHS peptide conjugation to CLIO-$NH_2$ increases MHEC uptake whereas combined peptide attachment and SIA modification results in the highest levels for VCAM-1 specific targeting. (**b**) FACS analysis of the starting material CLIO-$NH_2$ and the combined effects of peptide attachment and SIA modification of CLIO-$NH_2$ in macrophages. (**c**) FACS analysis of the starting material CLIO-$NH_2$ and the combined effects of peptide attachment and SIA modification of CLIO-$NH_2$ in endothelial cells. (**d**) Epifluorescence microscopy of VCAM-1–positive murine heart endothelial cells with fluorescence channel merged onto phase contrast images (mean ± s.d.). Scale bar, 10 μm.

nanoparticles allows efficient identification of binders that would otherwise be difficult to recover using small-molecule screens.

The small molecules used here were chosen to enable rapid synthesis and surface modifications. We believe that the efficacy of the described materials may be attributed to the multivalent nature of the surface molecules (60 ligands per nanoparticle). Multivalent interactions occur throughout biology and represent an evolutionary trend that exploits an existing pool of interactions rather than developing new ones. Multivalent drug design has yielded anti-inflammatory and antiviral agents several orders of magnitude more potent than monovalent agents[23]. Our results are in line with these observations and show that nanoparticle uptake can be increased by several orders of magnitude.

A logical extension of this work would be the attachment of novel complex small molecules with defined biological properties and specific protein binding[24]. Recent advances in diversity-oriented synthesis have allowed the creation of libraries of molecules that resemble natural products in their complexity and possess significant skeletal and stereochemical diversity[24]. Attachment of such libraries to nanoparticles in array could further extend the diversity of nanomaterials. Finally, the approach could be used not only to screen for novel binders but also to optimize linkers, spacers and conjugation chemistry, and to modulate pharmacokinetics and recognition by the reticuloendothelial system (e.g., for uptake in liver and spleen). Although this study used only one type of biocompatible nanoparticle preparation (dextran-coated nanoparticles), it is likely that the approach would work with other types of nanoparticle preparations as long as biocompatibility, appropriate pharmacokinetics and a capacity for multivalency are ensured. A number of synthetic biocompatible nanoparticles that could serve as base materials for new libraries have recently been described[21]. At least 5 (and preferably 20–100) such functionalities should be incorporated into the design to harness the multivalency of small ligands[23].

The application of such small-molecule approaches to generating nanomaterials offers the promise of generalized, higher-throughput methods to make novel nanomaterials useful in the diagnosis and treatment of disease. We expect that this union between nanotechnology and small-molecule chemistry will lead to the development of a wide range of novel nanomaterials for biomedical applications.

## METHODS

**Chemicals.** EDC (1-ethyl-3-(3-dimethylaminopropyl) carbodiimide hydrochloride), sulfo-NHS (sulfosuccinimidyl ester), SPDP (N-succinimidyl 3-(2-pyridyldithio) propionate) and SIA (succinimidyl iodo acetate) were purchased from Pierce. Cy5.5 NHS ester was obtained from Amersham. All other chemicals were purchased from Sigma Aldrich and used as received.

**Nanoparticle synthesis.** The nanoparticle used in this study was a monocrystalline magnetic nanoparticle[25], with a 3-nm core of $(Fe_2O_3)_n(Fe_3O_4)_m$ covered with a layer of 10 kDa dextran, that was cross-linked with epichlorohydrin and aminated by reaction with ammonia to provide primary amine groups (CLIO-$NH_2$)[26]. The nanoparticle had an overall size (volume weighted)

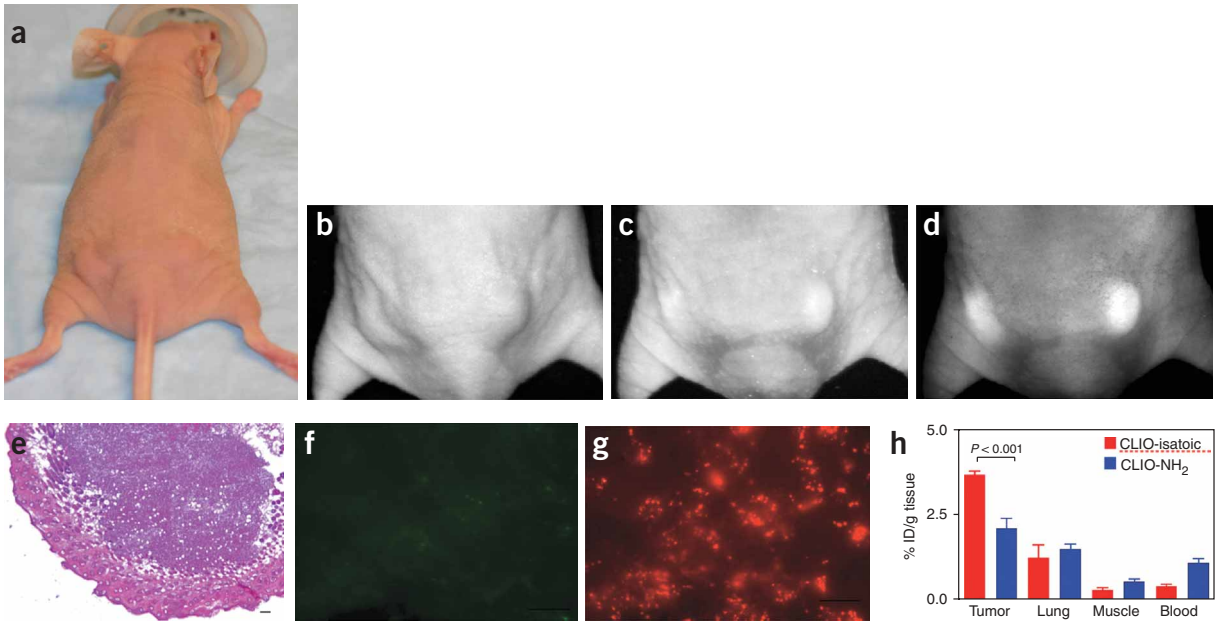


**Figure 5** *In vivo* targeting experiments. (**a**–**h**) PaCa-2 tumors were implanted bilaterally into the hind flanks of nude mice. Mice were injected intravenously with CLIO-Cy3.5 and CLIO-isoatoic-Cy5.5 (1 mg/kg). (**b**–**d**) White light excitation (**b**), Cy3.5 fluorescence channel (**c**) (recording on CLIO-Cy3.5) and Cy5.5 fluorescence channel (**d**) (recording on CLIO-isatoic-Cy5.5) generated raw black and white images. Note the prominent accumulation of CLIO-isoatoic-Cy5.5 in the bilateral pancreatic tumors indicating tumoral targeting. Hemotoxylin eosin–stained sections of the tumor (**e**). Cryotome sections observed using the Cy3.5 fluorescence channel indicate near-baseline levels of CLIO-Cy3.5 (**f**). Cryotome sections observed using the Cy5.5 fluorescence channel indicate marked fluorescence of CLIO-isatoic within tumor cells (**g**). Biodistribution study with $^{111}$In-labeled nanoparticles confirms tumoral targeting of CLIO-isatoic (**h**). Scale bar, 10 μm.

in aqueous solution of 38 nm, an R1 of 21 $mMsec^{-1}$, an R2 of 62 $mMsec^{-1}$ (37 °C, 0.5 T) and had an average of 62 primary amines available for conjugation. Fluorescein isothiocyanate (FITC) or Cy5.5 NHS ester was dissolved in DMSO and reacted with CLIO-$NH_2$ to yield an average of two fluorochromes per nanoparticle. The final reaction product was purified on Sephadex G-25 columns and used for small-molecule conjugation.

**Conjugation of small molecules.** To conjugate anhydrides to CLIO-$NH_2$, 100 μl (50 mM) of the anhydride DMSO solution was added to 2.0 mg CLIO-$NH_2$ (200 μl of 5.0 mg Fe/ml) in citrate solution. This was followed by addition of 10 μl 1-M NaOH solution. To conjugate carboxyls, the CLIO-$NH_2$ solution was first exchanged with morpholinoethanesulfonic acid buffer, pH 6.0. The solution was then concentrated to 5.0 mg/ml. We added 100 μl (50 mM) carboxylic acid compound in DMSO to 200 μl of a CLIO-$NH_2$ MES solution. This was followed by the addition of 5 μmol EDC and 5 μmol sulfo-NHS in MES solution. To conjugate thiols, CLIO-$NH_2$ was first reacted with SPDP. We mixed 1.0 mg SPDP-derivatized CLIO-FITC in 200 μl PBS buffer, pH 7.4 with 100 μl thiol compound in DMSO (50 mM). To conjugate amines (including amino acids), CLIO-$NH_2$ was first reacted with succinic anhydride and purified by Sephadex G-25. We then prepared 200 μl aliquots containing 1.0 mg Fe in MES buffer, pH 6.0 and 10 mg EDC and 10 mg sulfo-NHS was added to this solution. All of the above reactions were allowed to proceed for 2–4 h 21 °C to maximize conversion of all amines. Unreacted small molecules were removed using Sephadex G-25 columns eluted with PBS buffer, pH 7.4. All materials were characterized by size measurements, relaxometry, amine content and mass spectrometry. For biodistribution studies, CLIO-$NH_2$ was modified with three to five DTPA groups per nanoparticle and subsequently modified with small molecules. The compounds were labeled with $^{111}$In and purified to >99%.

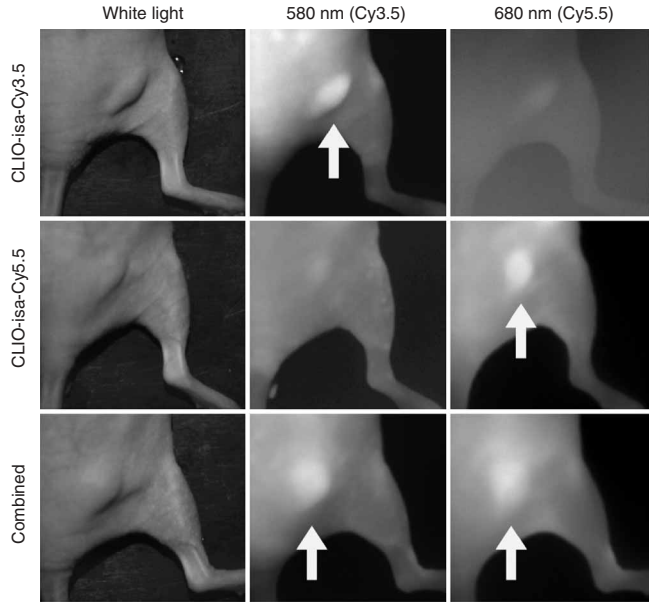


**Figure 6** *In vivo* targeting experiments similar to those described in **Figure 5** but with different fluorochrome-labeled nanoparticles (same acquisition parameters in each column). Note the accumulation of CLIO-isoatoic in the tumors irrespective of the fluorochrome used (arrows). Top row: CLIO-isatoic-Cy3.5, middle row: CLIO-isatoic-Cy5.5, bottom row: combined injection of CLIO-isatoic-Cy3.5 and CLIO-isatoic-Cy5.5.

**Cells.** U937 and PaCa-2 cells were obtained from the American Type Tissue Culture Collection (ATCC) and maintained according to ATCC protocols. For differentiation into macrophages, the nonadherent monocyte-like undifferentiated U937 cells were induced to differentiate by a 48-h exposure to 40 nM

phorbol-12-myristate-13-acetate (Sigma). After addition of PMA, cells were plated onto gelatin-coated 96-well tissue culture plates. Differentiated cells were maintained by replacement of PMA-containing media every 2–3 d.

Primary human macrophages were obtained from buffy coats. Briefly, mononuclear cells were isolated by density centrifugation using lymphocyte separation media (LSM; ICN Biomedicals) and the MACS human monocyte isolation kit (Miltenyi Biotec). Monocytes were plated onto cell culture–treated dishes and cultured in primary human monocyte medium containing RPMI 1640 1× with 10% fetal bovine serum, 10 ml/L 200 mM L-glutamine and 10 ml/L 10,000 IU/ml penicillin-streptomycin. Freshly isolated monocytes were treated to produce resting macrophages, GM-CSF–activated macrophages, foam cells and lipopolysaccharide S (LPS)-activated macrophages. To produce resting macrophages, cells were fed every 2–3 d while in culture. After 7 d, adherent cells were considered resting macrophages. GM-CSF–activated macrophages were prepared as follows: GM-CSF (stock solution 1 μg/ml) (BD Biosciences) was added to primary human monocyte medium at a dilution of 12 μl of GM-CSF solution per 1.0 ml of medium. The cells were maintained at this concentration of GM-CSF for 7 d before use in experiments. Foam cells were generated by treating primary human monocyte–derived macrophages with 10 μl of a 2 mg/ml stock solution of oxidized low-density lipoprotein (oxLDL, Biomedical Technologies) for 7 d before experiments. In addition, macrophages were treated with LPS for 24 h.

**Screening.** All cells were plated in 96-well plates. Cells were incubated with 0.1 mg/ml Fe of the indicated CLIO-derivatives for 4 h at 37 °C in the presence of 5% $CO_2$. After incubation, wells were washed 3× with PBS/0.1% BSA/0.05% Tween-20 wash buffer and then analyzed using fluorescence microscopy, flow cytometry or an immunoassay to quantify FITC concentration[27]. Microscopy was done using a Biorad 2000 confocal microscope or a Nikon 80i Eclipse microscope equipped with a 512 Photometrics Cascade CCD. Flow cytometry was performed using a Becton Dickinson FACSCalibur. All experiments were performed at least six times.

For each screening experiment, the uptake of FITC (pM) was $\log_{10}$ transformed, and the mean determined for each cell line. The resulting data were centered on the median and normalized by the standard deviation. The compounds were clustered with Cluster 3.0 using average linkage, and Euclidean distance as the similarity metric[28]. The heat map and the dendrogram of the clustered data were visualized using Java TreeView[29]. The color scale ranged from green (highest uptake) to black to red (lowest uptake).

***In vivo* experiments.** Selected fluorescence-labeled compounds were tested in a pancreatic adenocarcinoma xenograft mouse model after intravenous administration of different nanoparticle preparations (1 mg Fe/kg nanoparticle; $n = 16$ mice). Cohorts of mice received either (i) CLIO-isatoic-Cy3.5, (ii) CLIO-isatoic-Cy5.5 or (iii) mixtures of CLIO-isatoic-Cy3.5 and CLIO-isatoic-Cy5.5. Twenty-four hours later, animals were imaged using a fluorescence-imaging system (BonSai, Siemens) at different wavelengths, and values were expressed as ratios between the fluorochromes[10]. Tumoral fluorescence was calculated as tumor – background/background and values among different groups were compared using Student's *t*-test. Biodistribution experiments of DTPA-CLIO-$NH_2$-Cy3.5 and DTPA-CLIO-isatoic-Cy5.5 were performed in PaCa2-bearing mice ($n = 10$) following intravenous administration of $^{111}$In-labeled compounds (100 μl, 100 μCi/mouse). Organ distribution was expressed as % injected dose/g tissue.

*Note: Supplementary information is available on the Nature Biotechnology website.*

ACKNOWLEDGMENTS

The authors would like to acknowledge the help of Fred Reynolds for synthesizing the CLIO-peptide conjugates, Jan Grimm for radiolabelling, Terry O'Loughlin for molecular modeling and nanoparticle characterization and Jose-Luis Figueiredo, Rabi Upadhyay and Gregory Wojtkiewicz for technical assistance.

COMPETING INTERESTS STATEMENT

The authors declare that they have no competing financial interests.

Published online at http://www.nature.com/naturebiotechnology/
Reprints and permissions information is available online at http://npg.nature.com/reprintsandpermissions/

1. Whitesides, G.M. The 'right' size in nanobiotechnology. *Nat. Biotechnol.* **21**, 1161–1165 (2003).
2. Nam, J.M., Thaxton, C.S. & Mirkin, C.A. Nanoparticle-based bio-bar codes for the ultrasensitive detection of proteins. *Science* **301**, 1884–1886 (2003).
3. Tsapis, N., Bennett, D., Jackson, B., Weitz, D.A. & Edwards, D.A. Trojan particles: large porous carriers of nanoparticles for drug delivery. *Proc. Natl. Acad. Sci. USA* **99**, 12001–12005 (2002).
4. Gao, X. & Nie, S. Molecular profiling of single cells and tissue specimens with quantum dots. *Trends Biotechnol.* **21**, 371–373 (2003).
5. Zorov, D.B., Kobrinsky, E., Juhaszova, M. & Sollott, S.J. Examining intracellular organelle function using fluorescent probes: from animalcules to quantum dots. *Circ. Res.* **95**, 239–252 (2004).
6. Santra, S., Yang, H., Holloway, P.H., Stanley, J.T. & Mericle, R.A. Synthesis of water-dispersible fluorescent, radio-opaque, and paramagnetic CdS:Mn/ZnS quantum dots: a multifunctional probe for bioimaging. *J. Am. Chem. Soc.* **127**, 1656–1657 (2005).
7. Huber, M.M. *et al.* Fluorescently detectable magnetic resonance imaging agents. *Bioconjug. Chem.* **9**, 242–249 (1998).
8. Modo, M. *et al.* Mapping transplanted stem cell migration after a stroke: a serial, *in vivo* magnetic resonance imaging study. *Neuroimage* **21**, 311–317 (2004).
9. Josephson, L., Kircher, M.F., Mahmood, U., Tang, Y. & Weissleder, R. Near-infrared fluorescent nanoparticles as combined MR/optical imaging probes. *Bioconjug. Chem.* **13**, 554–560 (2002).
10. Kircher, M.F., Weissleder, R. & Josephson, L. A dual fluorochrome probe for imaging proteases. *Bioconjug. Chem.* **15**, 242–248 (2004).
11. Wu, Y., Xiang, J., Yang, C., Lu, W. & Lieber, C.M. Single-crystal metallic nanowires and metal/semiconductor nanowire heterostructures. *Nature* **430**, 61–65 (2004).
12. Kang, H.W., Josephson, L., Petrovsky, A., Weissleder, R. & Bogdanov, A., Jr. Magnetic resonance imaging of inducible E-selectin expression in human endothelial cell culture. *Bioconjug. Chem.* **13**, 122–127 (2002).
13. Hogemann, D., Ntziachristos, V., Josephson, L. & Weissleder, R. High throughput magnetic resonance imaging for evaluating targeted nanoparticle probes. *Bioconjug. Chem.* **13**, 116–121 (2002).
14. Akerman, M.E., Chan, W.C., Laakkonen, P., Bhatia, S.N. & Ruoslahti, E. Nanocrystal targeting *in vivo*. *Proc. Natl. Acad. Sci. USA* **99**, 12617–12621 (2002).
15. Kelly, K.A. *et al.* Detection of vascular adhesion molecule-1 expression using a novel multimodal nanoparticle. *Circ. Res.* **96**, 327–336 (2005).
16. Harisinghani, M.G. *et al.* Noninvasive detection of clinically occult lymph-node metastases in prostate cancer. *N. Engl. J. Med.* **348**, 2491–2499 (2003).
17. Boullier, A. *et al.* Scavenger receptors, oxidized LDL, and atherosclerosis. *Ann. NY Acad. Sci.* **947**, 214–222, discussion 222–213 (2001).
18. Denis, M.C., Mahmood, U., Benoist, C., Mathis, D. & Weissleder, R. Imaging inflammation of the pancreatic islets in type 1 diabetes. *Proc. Natl. Acad. Sci. USA* **101**, 12634–12639 (2004).
19. Libby, P. & Aikawa, M. Stabilization of atherosclerotic plaques: new mechanisms and clinical targets. *Nat. Med.* **8**, 1257–1262 (2002).
20. Pham, W., Kircher, M.F., Weissleder, R. & Tung, C.H. Enhancing membrane permeability by fatty acylation of oligoarginine peptides. *Chem. BioChem.* **5**, 1148–1151 (2004).
21. Anderson, D.G., Levenberg, S. & Langer, R. Nanoliter-scale synthesis of arrayed biomaterials and application to human embryonic stem cells. *Nat. Biotechnol.* **22**, 863–866 (2004).
22. Goodman, C.M., McCusker, C.D., Yilmaz, T. & Rotello, V.M. Toxicity of gold nanoparticles functionalized with cationic and anionic side chains. *Bioconjug. Chem.* **15**, 897–900 (2004).
23. Mammen, M., Chio, S-K. & Whitesides, G.M. Polyvalent interactions in biological systems: implications for design and use of multivalent ligands and inhibitors. *Angew. Chem. Int. Edn Engl.* **37**, 2755–2794 (1998).
24. Schreiber, S.L. Target-oriented and diversity-oriented organic synthesis in drug discovery. *Science* **287**, 1964–1969 (2000).
25. Shen, T., Weissleder, R., Papisov, M., Bogdanov, A., Jr. & Brady, T.J. Monocrystalline iron oxide nanocompounds (MION): physicochemical properties. *Magn. Reson. Med.* **29**, 599–604 (1993).
26. Wunderbaldinger, P., Josephson, L. & Weissleder, R. Crosslinked iron oxides (CLIO): a new platform for the development of targeted MR contrast agents. *Acad. Radiol.* (suppl. 2) **9**, S304–S306 (2002).
27. Kelly, K.A., Reynolds, F., Weissleder, R. & Josephson, L. Fluorescein isothiocyanate-hapten immunoassay for determination of peptide-cell interactions. *Anal. Biochem.* **330**, 181–185 (2004).
28. de Hoon, M.J., Imoto, S., Nolan, J. & Miyano, S. Open source clustering software. *Bioinformatics* **20**, 1453–1454 (2004).
29. Saldanha, A.J. Java Treeview—extensible visualization of microarray data. *Bioinformatics* **20**, 3246–3248 (2004).